*Materials Research*. 2022; 25:e20210339
DOI: https://doi.org/10.1590/1980-5373-MR-2021-0339

# Effect of Hydrogen on the Mechanical Properties of ASTM A182 F22 and ASTM A36 Steels Welded Joint Using Inconel 625 as Filler and Buttering Metal

*Adiana Nascimento Silva*[a]*, *Esdras Carvalho Costa*[b], *José Gonçalves de Almeida*[c], *Theophilo Moura Maciel*[c], *Danielle Guedes de Lima Cavalcante*[d], *Tibério Andrade dos Passos*[d]

[a]*Universidade Federal Rural do Semi-Árido - UFERSA, Departamento de Engenharias, Caraúbas, RN, Brasil.*
[b]*Universidade Federal da Paraíba - UFPB, Programa de Pós-graduação em Engenharia Mecânica, João Pessoa, PB, Brasil.*
[c]*Universidade Federal da Paraíba - UFPB, Departamento de Engenharia de Mecânica, João Pessoa, PB, Brasil.*
[d]*Universidade Federal da Paraíba - UFPB, Departamento de Engenharia de Materiais, João Pessoa, PB, Brasil.*

Received: July 05, 2021; Revised: December 29, 2021; Accepted: January 13, 2022

ASTM A 182 F22 steel, used in components subsea for oil extraction, are previously buttered with ductile metal such as Inconel 625, before being welded to steel pipes similar to ASTM A36 steels. The thermal buttering weld cycle provides the formation of high hardness micro-phases and carbides at the interface between F22 steel and the buttering with Inconel, which when in contact with hydrogen, originating from the cathodic protection applied to these equipment, can lead to the embrittlement of this region, causing fragile fractures. In this work, ASTM A 182 F22 steel, buttered with Inconel 625 and welded to A36 steel, submitted to post-weld heat treatment without hydrogenation and subjected to cathodic protection for hydrogen permeation were submitted to fracture toughness test. The welds and buttering were done using GMAW process with AWS ERNiCrMo-3 wire as filler and buttering metal and a mixture of Ar and He as shield gas. The results indicated a 56% of area reduction, and 15% in the elongation values in the tensile tests, in addition to a 13.3% reduction in the CTOD value, for welded joints subjected to hydrogen permeation, which showed a quasi-cleavage fracture mechanism.

**Keywords**: *ASTM A182 F22 steel, Inconel 625, Welded joints, Hydrogen embrittlement, Mechanical Properties.*

## 1. Introduction

The manifold is a control component that plays a crucial role in offshore oil exploration. This equipment made of forged steels, such as ASTM A182 F22 steel, arrives at sea in a pre-assembled state in order to facilitate field assembly and be welded to pipeline made of most malleable steel, such as ASTM A36 steel. Before welding, the part of this equipment, which will be joined to the pipelines, is previously subjected to a deposition of welding passes, named buttering, using Ni alloys such as Inconel 625, in order to reduce the effect caused by the welding thermal cycle on the heat affected zone (HAZ) in view of the dissimilarity of between steel and nickel alloy[1]. Partially mixed zones (PMZs) and carbides can reach high hardness values, compromising the toughness of this region[2], involving carbon-rich microphases[3] even after the application of post-weld heat treatment (PWHT)[4].

After welding, this equipment undergoes a continuous cathodic protection process, thus guaranteeing a minimum of corrosion deterioration during its useful life[5]. In this protection, forced current flow is used to provide the potential for polarization through a galvanic electrochemical reaction[6]. However, this process provides hydrogen ion reduction reactions. This element is absorbed and diffuses into the metal due to its solubility in the metallic network, concentrating in voids and microstructural defects, and, in regions of high hardness such as PMZs, making the region of the interface between the buttering and the alloy of Ni and forged steel, very brittle and susceptible to fracture[7].

This paper aims to evaluate the susceptibility to hydrogen embrittlement in the region of the interface between a buttering with the Inconel 625 alloy, and the ASTM A 182 F22 forged steel through tensile tests, with the useful part of the specimens containing the interface of the weld, and fracture toughness test using specimens for CTOD (crack tip opening displacement) with the notch locate 1 mm from the interface region. Both tested were done with (WH) and without (OH) the application of polarization potential for hydrogen generation.

## 2. Experimental Procedure

ASTM A182 F22 steel used in the present study was supplied in the form of a forged billet with dimensions 215 x 25.4 mm for diameter and height, respectively, which

*e-mail: adianans@gmail.com

was sectioned into two sheets with dimensions of 180 x 76 mm x 25.4 mm. The chemical composition and mechanical properties of steel, were raised, respectively, through Optical Emission Spectroscopy (OES) and mechanical tests (Hardness and Traction), whose results are shown in Tables 1 and 2.

The other base metal used in the formation of the welded joint, representing the metal of the pipes, was ASTM A36 steel, obtained in the form of a rolled sheet, with a thickness of 25.4mm and cut in the same dimensions as the sheets of ASTM A182 F22 steel.

The welding process used was the Gas Metal Arc Welding (GMAW). This process was used both in the buttering of ASTM A182 F22 steel and in obtaining of welded joints. The shielding gas used was a mixture between Argon and Helium, in the proportions of 75% and 25% respectively. The filler metal used for buttering and weld process was the solid wire AWS ERNiCrMo-3 (Ni-based Alloy 625) with a diameter of 1.2 mm, whose chemical composition, according to the manufacturer, is specified in Table 3. The mechanical properties of the weld metal extracted from the weld joint, ASTM A182 F22 steel - Ni 625 alloy - ASTM A36 steel, are in accordance with the criteria AWS A5.14: ERNiCr Mo-3, and are elucidated in Table 4.

In Figure 1, there is a diagram showing part of the buttering weld, through which the arrangement of eight weld bead arranged in two layers is observed. In Figure 1a, the welding sequence adopted in this weld is verified, whose welds were arranged in parallel, along the thickness. Figure 1b shows the cross section of buttered steel. The welding parameters for executing the weld beads are shown in Table 5, both in the butter and in the welded joint used the GMAW conventional process with voltage adjustment.

**Table 1.** Chemical composition (in weight percent), of ASTM A182 F22 steel.

| C | Si | Mn | P | S | Ni | Cr | Mo | Cu | Al |
|---|---|---|---|---|---|---|---|---|---|
| 0.17 | 0.14 | 0.35 | 0.01 | 0.01 | 0.04 | 2.11 | 0.93 | 0.04 | 0.30 |

**Table 2.** Average values of the mechanical properties of ASTM A182 F22 steel as received.

| Hardness (HRC) | Yield Stress (MPa) | Tensile Strength Limit (MPa) | Elongation (%) |
|---|---|---|---|
| 28.5 | 877 | 960 | 22 |

**Table 3.** Chemical composition (in weight percent), of the wire AWS ERNiCrMo-3 (manufacturer).

| Ni | Cr | Mo | C | Fe | Al | Nb | Si | Mn |
|---|---|---|---|---|---|---|---|---|
| 64.31 | 22.34 | 9.13 | 0.01 | 0.19 | 0.09 | 3.51 | 0.06 | 0.01 |
| P | S | Co | Ti | Cu | Mg | Pb | Ta | N |
| 0.003 | 0.001 | 0.03 | 0.21 | <0.01 | 0.009 | <0.001 | 0.02 | 0.02 |

**Table 4.** Mechanical properties of the weld metal AWS ERNiCrMo-3.

| Yield Stress (MPa) | Ultimate Tensile Strength (MPa) | Elongation (%) |
|---|---|---|
| 468 | 758 | 64 |

**Table 5.** Buttering weld parameters.

| Preheat temperature (ºC) | Current (A) | Voltage (V) | Wire feeding speed (m/min) | Welding speed (m/min) | Heat Input (kJ/mm) |
|---|---|---|---|---|---|
| ≈300 | 199.87 | 25.85 | 7 | 0.21 | 1.48 |

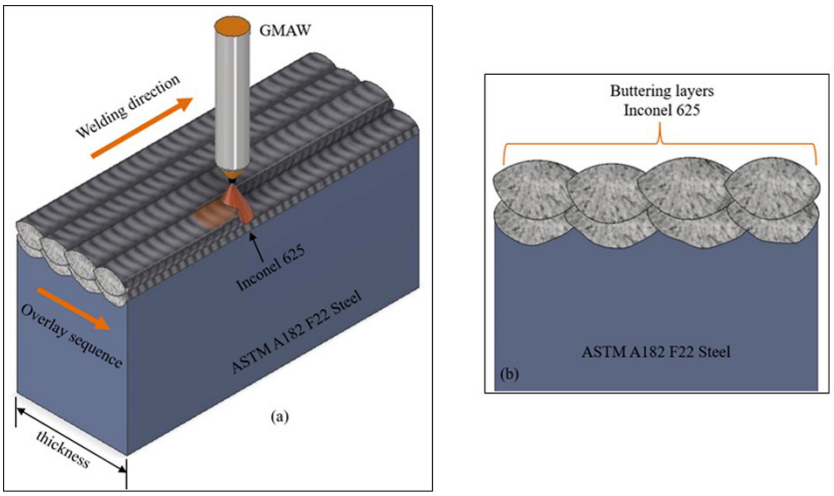


**Figure 1.** Buttering weld. Procedure (a) and its transversal section (b).

This buttering consisted of a total of 16 weld beads, which were distributed in four layers composed of four beads. The total overlapping of the buttering layers allowed a thickness of 9.5 mm, which can be seen in Figure 2.

After applying the buttering, the set was subjected to post-weld heat treatment (PWHT). Time was used which, from a practical point of view, was feasible and at the same time sufficient to guarantee the reduction in the level of hardness that is specified by the NACE MR0175 standard for subsea applications. Oliveira[8] found that, for a two hour PWHT, the hardness levels were practically unchanged. In turn, Dodge[9] obtained interesting results using a ten hour PWHT. Then, in the interest of the present research, the time of six hours was defined at a plateau temperature of 677 ºC, was defined for relieve residual stresses from buttering weld composed of ASTM A182 F22 and Inconel 625 steel. The buttered material composed the dissimilar joint, ASTM A182 F22 steel - Inconel 625 - ASTM A36 steel, whose performance in the presence of hydrogen was evaluated. The PWHT parameters are shown in Table 6.

After rectification, the welded joint was performed, using nine welding passes with the parameters showed in Table 7.

Figure 2 shows an illustration of the buttered ASTM A182 F22 steel welded to ASTM A 36 steel. The Figure also shows the arrangement of the specimens for the tensile tests.

In order to evaluate the microstructure of the welded joint, samples from the interface region between ASTM F22 steel and Inconel 625 were subjected to analysis by optical microscopy (OM) and scanning electron microscopy (SEM). The specimen were polished with, 3 and 1/4μm diamond paste and etched by immersion in 2% nital solution, for 20s, in order to reveal the ASTM A182 F22 steel microstructure, afterwards an electrolytic etching was carried out with 10% chromic acid for a 5V voltage lasting 30s, which allowed the visualization of the microstructure of the Inconel 625. For analysis by electron microscopy, a LEO 1430 electron microscope with secondary electron detector (SE) was used.

Microhardness tests were performed using a Shimadzu equipment model HMV – 2, with a load of 100gf ($HV_{0.1}$) for 15s. In Figure 3, there is the demonstrative scheme of the test procedure, which corresponded to 09 columns, grouped 03 by 03, totaling 186 indentations per group. The distance between the impressions of the same column was 0.5 mm, as shown in Figure 3. From the five highlighted indentations, an average value was taken which corresponded to a point on the hardness profile curve.

The tensile tests were performed on a 200kN Shimadzu Servo Pulser model. The dimensions of the specimen and other test parameters followed the recommendations of the ASTM standard[10]. The loading speed used was 0.6 mm/min. The ilustration of the specimen for the tensile test containing the interface and the F22 steel removed from the welded joint is showed in details in Figure 4.

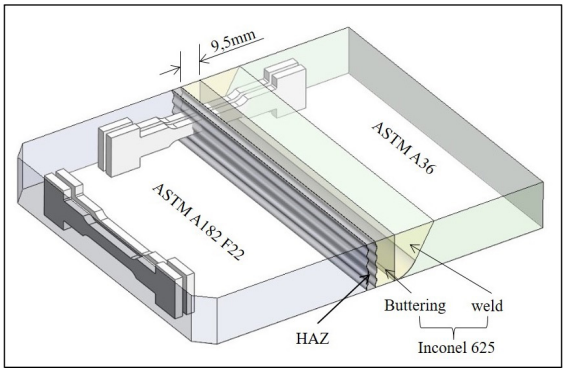


**Figure 2.** Dissimilar ASTM A183 F22 steel – Inconel 625 –ASTM A36 steel, welded joint showing the extraction direction of the tensile test specimens.

**Table 6.** PWHT parameters.

| | |
|---|---|
| Heating rate | 20 ºC/min |
| Temperature | 677 ºC ± 10ºC |
| Stability time | 6 h |
| Cooling | calm air |

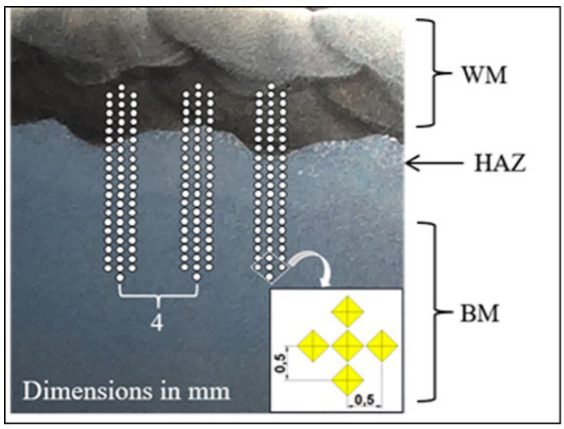


**Figure 3.** Distribution of indentations in the microhardness test.

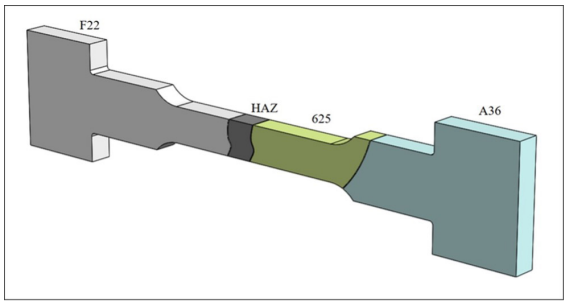


**Figure 4.** Tension specimen of the welded joint[11].

**Table 7.** Welding procedure parameters.

| Preheat temperature (ºC) | Current (A) | Voltage (V) | Wire feeding speed (m/min) | Welding speed (m/min) | Heat Input (kJ/mm) |
|---|---|---|---|---|---|
| ≈300 | 174.71 | 24.95 | 7 | 0.21 | 1.25 |

For the performance of fracture toughness tests, a three-point bending test apparatus was used, with specimen of type SE (B), which were machined according to the standard[12] (See Figure 5). The position of the groove and the fatigue crack were approximately 1mm from the interface between ASTM A 182 F22 steel and the buttering with Inconel 625, as shown in Figure 6.

All conditions established by the standard for validation of CTOD were met, among which the following stand out:

- the a / W ratio is between 0.45 and 0.70;
- the difference between any of the seven central points and the length of crack a, does not exceed 0.1 * a;
- a ≥ 1.3 mm or 2.5% W, whichever is greater, the parameter CTOD (δ) was calculated using Equation 1[12].

$$\delta = \left[\frac{FS}{BW^{1,5}} xf\left(\frac{a_0}{W}\right)\right]^2 \frac{\left(1-\nu^2\right)}{2\sigma_{YS}E} + \frac{0,4\left(W-a_0\right)V_P}{0,4W+0,6a_0+z} \quad (1)$$

Where Vp is the plastic component of the Force x Notch Opening Displacement (NOD) obtained in the test.

For the hydrogen permeation process in the specimens, simulating cathodic protection, using the recommendations of[13] were followed. The NaCl solution, with a mass concentration of 35.00 g / L, was used to simulate sea water. In the cathodic protection apparatus of the printed current type, Figure 7, there is a reservoir, where the solution was disposed, together with the specimen to be protected (cathode - negative terminal) and the titanium plates (anode - positive terminal), as well as a voltage supply that comes from a direct current electrical source.

In the hydrogen production process, pH 7 (neutral) and loading temperature of 0 °C was adopted for a period of 07 days, with a potential of -1.100 m $V_{SCE}$, as shown in Table 8.

## 3. Results and Discussion

### *3.1. Macro and microstructural analyzes*

Figure 8 shows the image of the interface between the buttering weld and the base metal, the region of which is homogeneous and free from discontinuities. It can also be

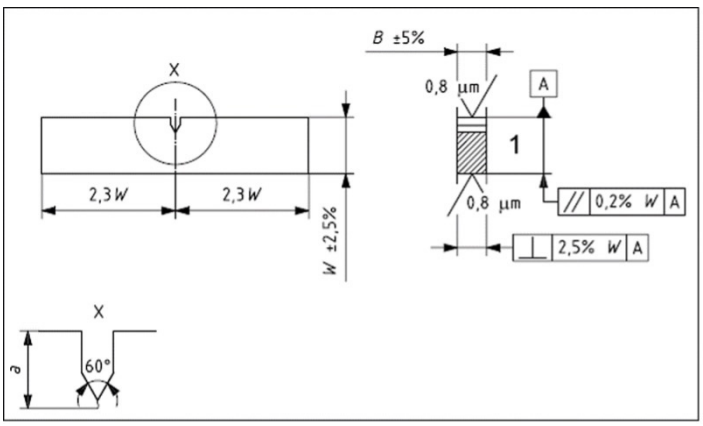


**Figure 5.** Dimension and tolerances of CTOD specimen, test[12].

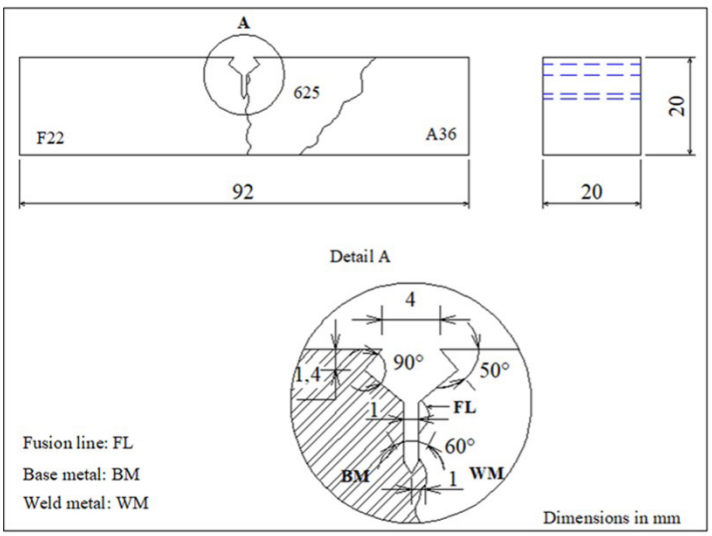


**Figure 6.** Location of the fatigue pré-crack in CTOD welded joint specimens.

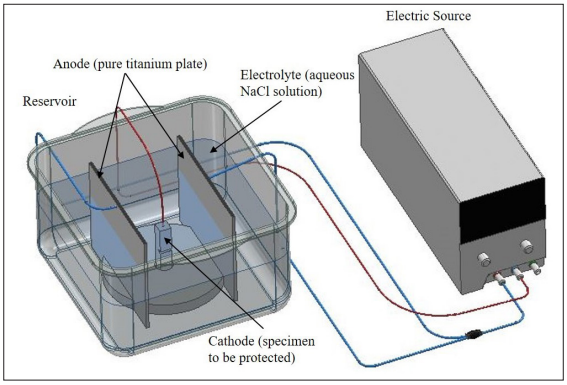


**Figure 7.** Cathodic protection apparatus.

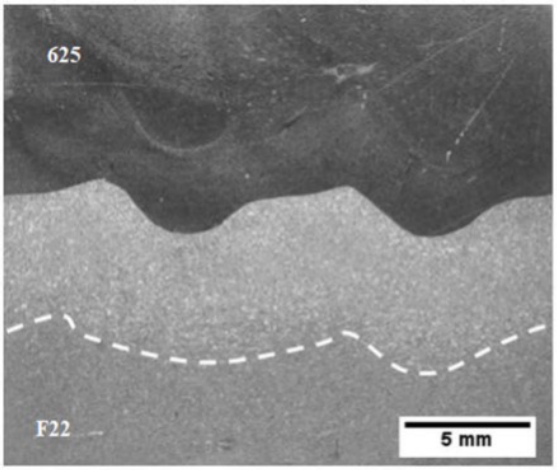


**Figure 8.** Buttering weld interface as-welded.

observed that the heat affected zone (HAZ), the lightest region, outlined by the dashed line, wich presented an extension varying between approximately 4 and 5 mm.

In the images of Figures 9 and 10, there is the microstructure of the buttering weld interface, in which the partially mixed zones (PMZs) are observed, identified at the interface between the Ni layer and the steel. In this dissimilar interface, zones Δ, ϕ, Π, M and "swirls" and "islands" types are commonly found. The Δ zone, indicated by the dashed line in Figure 9a, contained in the coarse-grained region of the steel HAZ, is basically made up of depleted C ferrite due to the diffusion of this element to Ni[14]. Zone ϕ, shown in Figure 9b, is a high hardness Ni solid solution supersaturated of carbon diffused from steel, and, therefore, a region conducive to embrittlement, since the carbides present there, such as those from type $Cr_7C_3$ can act as hydrogen trapping sites[15]. The ϕ zone was uniform and approximately 10 μm in size.

Figure 9b also shows the cell dendritic zone (Π), located above zone Φ on the side of Inconel 625. Zone Π is formed due to a change in the solidification rate and temperature gradient[16]. The cellular dendritic structure tends to have carbides rich in Nb and Mo that decorate the dendritic boundaries[17].

Figure 10a and b, shows images extracted by the LAMS technique[18], showing macrosegregations of "island" and "swirl" type, with some of the microhardness values surveyed at the dissimilar interface, which is also shown in Table 9. Within the red rectangle of Figure 10b, there are dark regions, on the steel side, known as M zones. These zones are characterized by microstructural similarity with the base metal, having a very significant presence of martensite. Among the forms of presentation of zone M, Figures 9b and 10, a predominance of the types "beaches" and "swirl" was observed. The authors Dodge et al.[15] mention that the amount of this type of

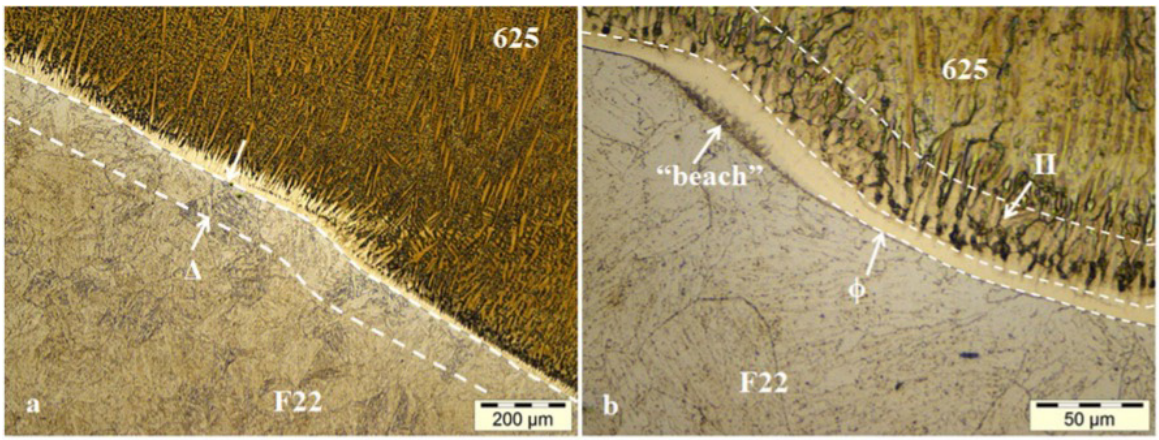


**Figure 9.** Microstructure of the buttering weld interface. (a) 100x. (b) 500x.

**Table 8.** Cathodic protection parameters.

| Electrolyte | Protection potential | Inert anode | Reference electrode | Continuous hydrogenation time |
|---|---|---|---|---|
| NaCl at 0ºC and pH 7 | -1.100mV$_{SCE}$ | Pure titanium plate | Calomel type | 168 hours |

formation is due to the welding parameters. Figure 10c and d correspond to SEM images of the M region, contained within the red rectangle, in which elongated microstructures are seen, suggestive of the martensitic microstructure. It can be also seen that the Vickers microhardness values in this microstructure (Figure 10b) and Table 9), were approximately 400 $HV_{0.1}$, which are compatible with this type of formation. The authors Frei et al.[19] observed hardness values of the same order of magnitude in the ASTM A182 grade 22 steel HAZ, which were associated with virgin martensite. The authors Dai and Lippold[20] also observed the presence of those virgin martensite in the PMZs of 8630 steel samples buttered with Inconel 625 and treated above 600°C. This formation is justified by the occurrence of austenitic transformation during PWHT. They found that, even at very low cooling rates, this martensite is formed and exhibited levels of hardness around 330 to 450 VHN. Fenske et al.[21], mention that the high Ni content can reduce the $A_{C1}$ temperature, making it lower than the PWHT temperature, favoring reaustenitize in discontinuous PMZs with microstructure of the base metal, and, consequently, generating virgin martensite after cooling. The high hardness of martensite makes it more susceptible to embrittlement by hydrogen. When the martensitic transformation occurs, the residual stress and the number of displacements increase. This will lead to a greater volume of capture sites, which will decrease the rate of diffusion and increase the concentration of hydrogen.

**Table 9.** Average values and standard deviation of microhardness tests ($HV_{0.1}$).

| Zones | With PWHT |
|---|---|
| Δ | 240.4 ± 21.6 |
| ϕ | 260.5 ± 31.6 |
| Π | 285.5 ± 42.3 |
| M | 404 ± 38.6 |

Figure 11 shows the average values of Vickers microhardness and the respective standard deviations for the regions of the weld metal (WM), which corresponds to the molten region, the HAZ and the base metal of the welded joint F22 - Inconel 625 - A36. In the abscissa axis there is the distance, in milimeters, from the region analyzed in relation to the fusion line. It is important to highlight that the hardness values presented previously, in Table 9, are not included in Figure 11. The materials applied in the production of oil and gas, with environments containing $H_2S$, must meet, among other criteria, the hardness levels established by the standard[22], in order to reduce the risk of hydrogen embrittlement. This standard establishes that, after PWHT, the hardness in BM and HAZ must be less than 250HV. The BM and HAZ regions (Figure 11) present, in a global way (Table of Figure 11), average hardness values that meet the NACE standard.

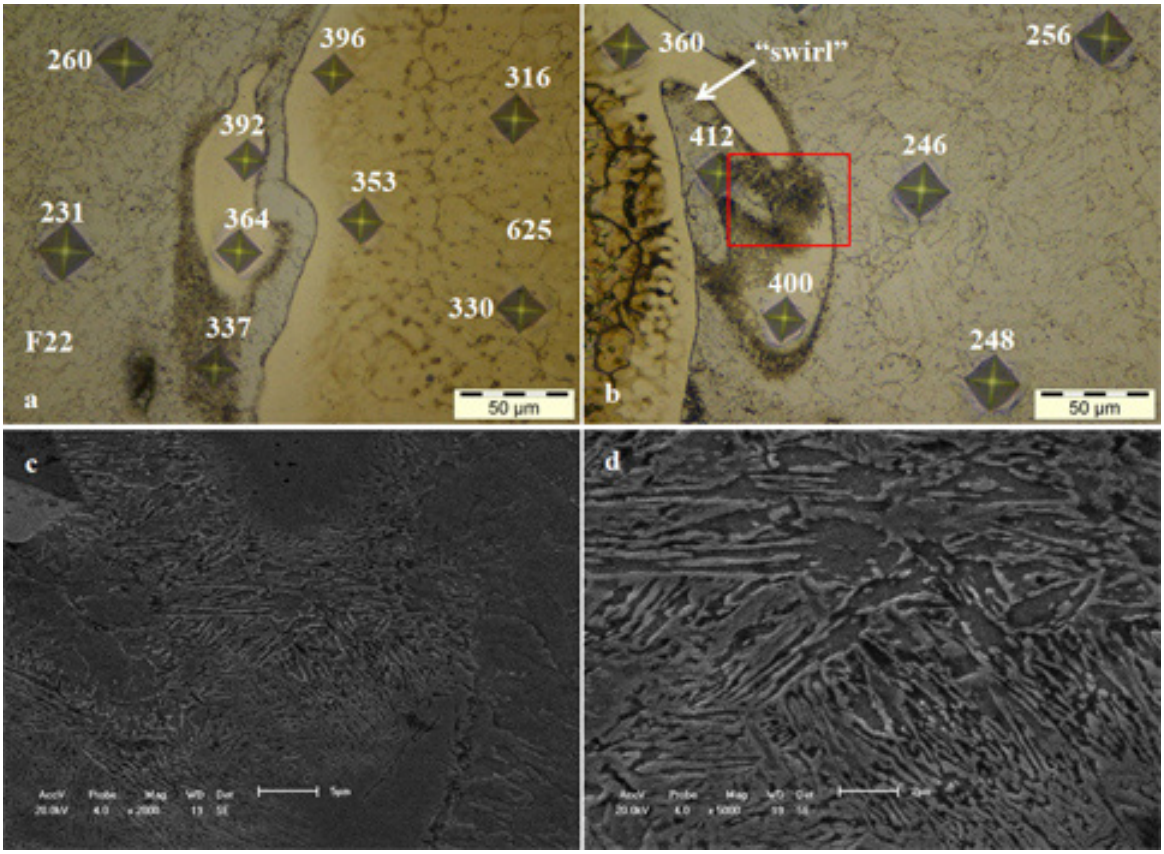


**Figure 10.** Buttering weld. (a) OM from "islands " (500x). (b) OM from "swirl" (500x). (c) e (d) SEM of the region comprised by the red rectangle, respectively, (2000x) e (5000x).

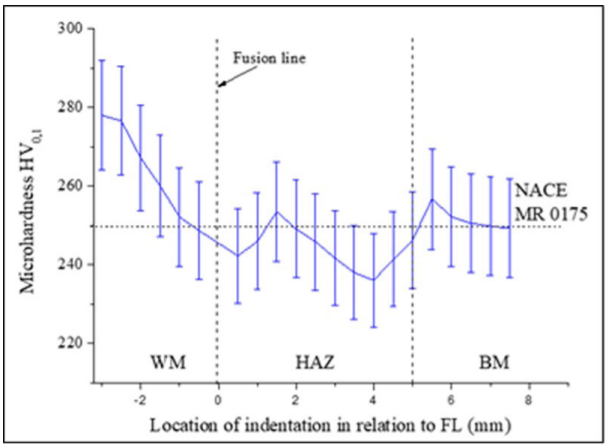


| Region | Welded joint |
|---|---|
| WM | 263.8 ± 12.29 |
| HAZ | 244.1 ± 5.75 |
| BM | 249.9 ± 4.59 |

**Figure 11.** Average Vickers microhardness profiles of the WM, HAZ and BM regions.

### *3.2. Tensile test*

The average stress-strain curves of ASTM A182 F22 steel and the welded joint, in conditions without and with the presence of hydrogen, introduced by cathodic protection, are shown in Figures 12 and 13, respectively. Considering the base metal, it appears that the curves have similar behaviors, that is, the elongation, the area reduction and the flow limits and tensile strength, have not changed with the presence of hydrogen, as can be confirmed through Table 10 and Figure 12, as well as by calculating the fragility index (Fi), which is the relationship between deformations with (WH) and without (OH) the presence of hydrogen presented in Equation 2. It was shown that the value was close to 1 for the base metal.

$$Fi = \varepsilon_H / \varepsilon = 23.87 / 23.13 = 1.03 \quad (2)$$

Figure 13 shows that, for the welded joint specimens, there was a significant difference in the shape of the curves with regard to ductility. The hydrogenated specimens showed a significant reduction in ductility, as can be seen in Table 11 and by the $F_I$ value which was equal to 0.85. In addition, all fractures occurred in the vicinity of the fusion line, region with presence of the PMZs that, as verified, have high hardness values, especially those regions close to zone M and ϕ, as shown in Figure 10 and Table 9. This result ensures that, even with the HAZ presenting a average hardness value of the order of 266$HV_{0.1}$, 1.5 mm from the fusion line (chart in Figure 11), the microphases present, close to this region, as the M zones (Figure 10 and Table 9) were responsible for susceptibility to hydrogen embrittlement.

On the other hand, it is observed that the values of the yield and tensile strength limits have practically not changed due to the presence of hydrogen. This result was already expected, as it has been observed that the phenomenon of hydrogen embrittlement acts more in the process of reducing ductility and fracture toughness[23].

The deformation results are consistent with the fractographs, which are presented in Figures 14 and 15, for the test specimens of the base metal and the welded joint, respectively. Through Figure 14, it can be seen that the samples of the base metal without and with hydrogenation

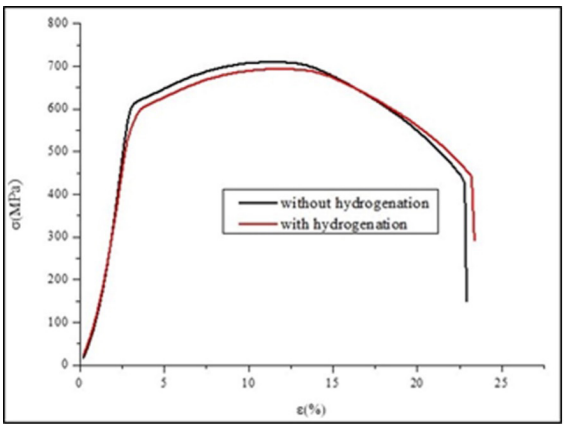


**Figure 12.** Results of tensile test of ASTM A182 F22 steel extracted from the welded joint without and with hydrogenation.

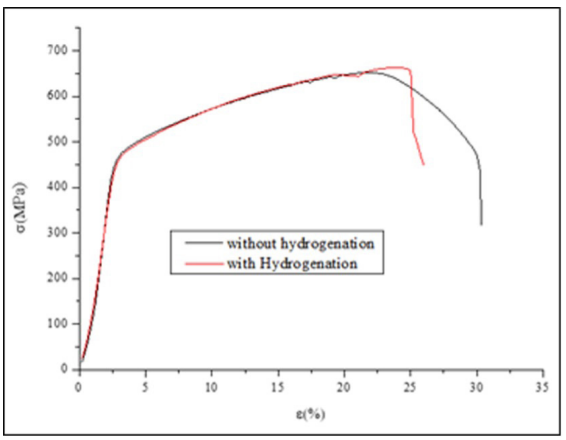


**Figure 13.** Results of tensile test of welded joint without and with hydrogenation.

presented fracture morphology typically ductile with microvoid coalescence (dimples).

The presence of a typically ductile fracture mechanism, with microvoid coalescence (dimples), was also observed for the welded joint without hydrogenation, Figure 15a. Regarding

**Table 10.** Mechanical properties of the base metal (ASTM A182 F22 steel) without (OH) and with (WH) hydrogenation.

| Condition | Specimen | Yield Limit $R_{p0.2}$ (MPa) | Tensile Strength Limit $\sigma_{rt}$ (MPa) | Strain (%) | Area Reduction (%) |
|---|---|---|---|---|---|
| OH | 1 | 629.15 | 718.57 | 23.80 | 60.00 |
| | 2 | 615.65 | 704.63 | 22.80 | 58.33 |
| | 3 | 616.92 | 707.75 | 22.80 | 59.38 |
| | **Average** | **620.57** | **710.32** | **23.13** | **59.24** |
| WH | 1 | 591.99 | 686.77 | 23.60 | 63.58 |
| | 2 | 621.15 | 702.87 | 24.80 | 62.54 |
| | 3 | 600.37 | 693.30 | 23.20 | 65.17 |
| | **Average** | **604.50** | **694.31** | **23.87** | **59.17** |

**Table 11.** Mechanical properties of the welded joint, steel ASTM A182 F22 - Inconel 625 - steel ASTM A36, without (OH) and with (WH) hydrogenation.

| Condition | Specimen | Yield Limit $R_{p0.2}$ (MPa) | Tensile Strength Limit $\sigma_{rt}$ (MPa) | Strain (%) | Area Reduction (%) |
|---|---|---|---|---|---|
| OH | 1 | 450.90 | 651.04 | 30.80 | 61.67 |
| | 2 | 462.76 | 655.86 | 31.60 | 58.33 |
| | 3 | 466.58 | 653.57 | 30.20 | 62.62 |
| | **Average** | **460.08** | **653.49** | **30.87** | **60.87** |
| WH | 1 | 461.82 | 657.68 | 26.40 | 28.50 |
| | 2 | 451.72 | 669.24 | 27.60 | 28.50 |
| | 3 | 458.80 | 668.95 | 25.00 | 23.50 |
| | **Average** | **457.44** | **665.29** | **26.33** | **26.83** |

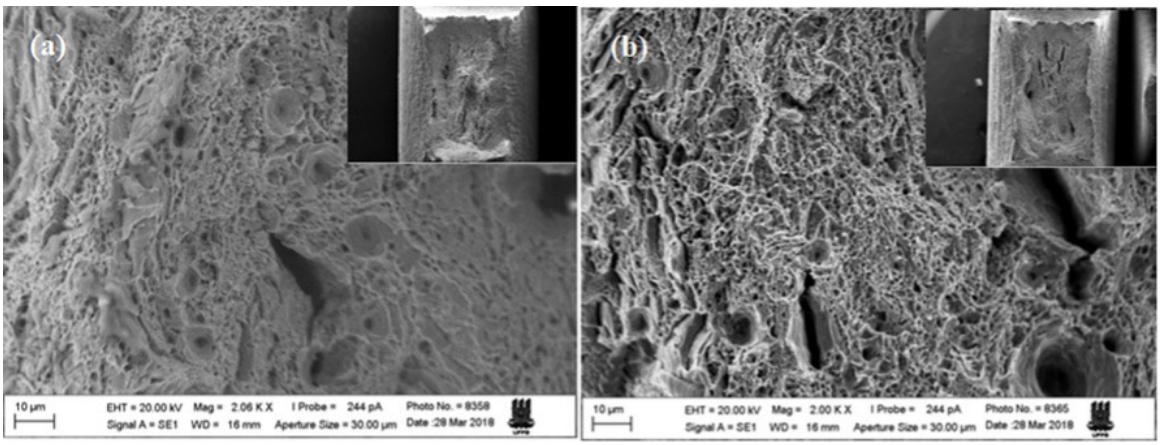


**Figure 14.** Fractography of the tensile test of forged ASTM A182 F22 steel, extracted from the joint. (a) without. (b) with hydrogenation.

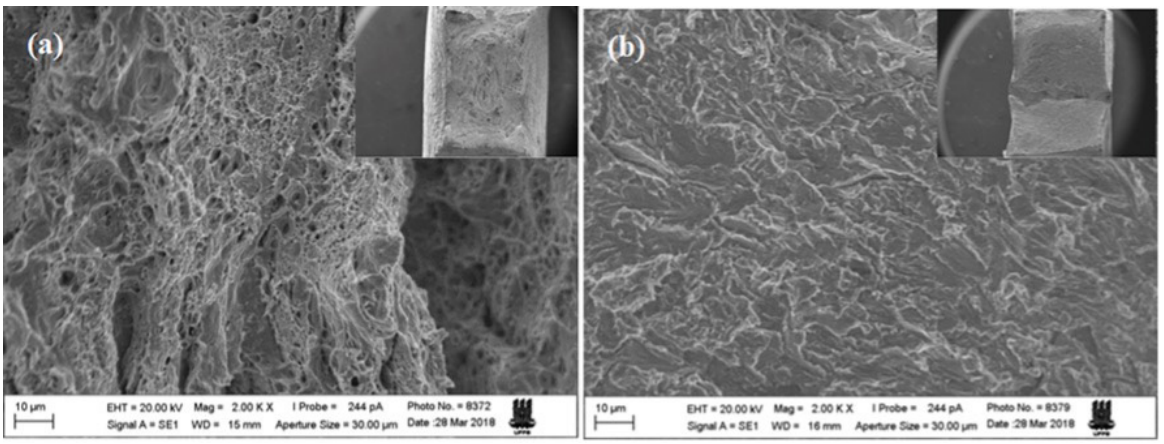


**Figure 15.** Fractography of the tensile test of the welded joint steel ASTM A182 F22 - Inconel 625 - steel ASTM A36. (a) without. (b) with hydrogenation.

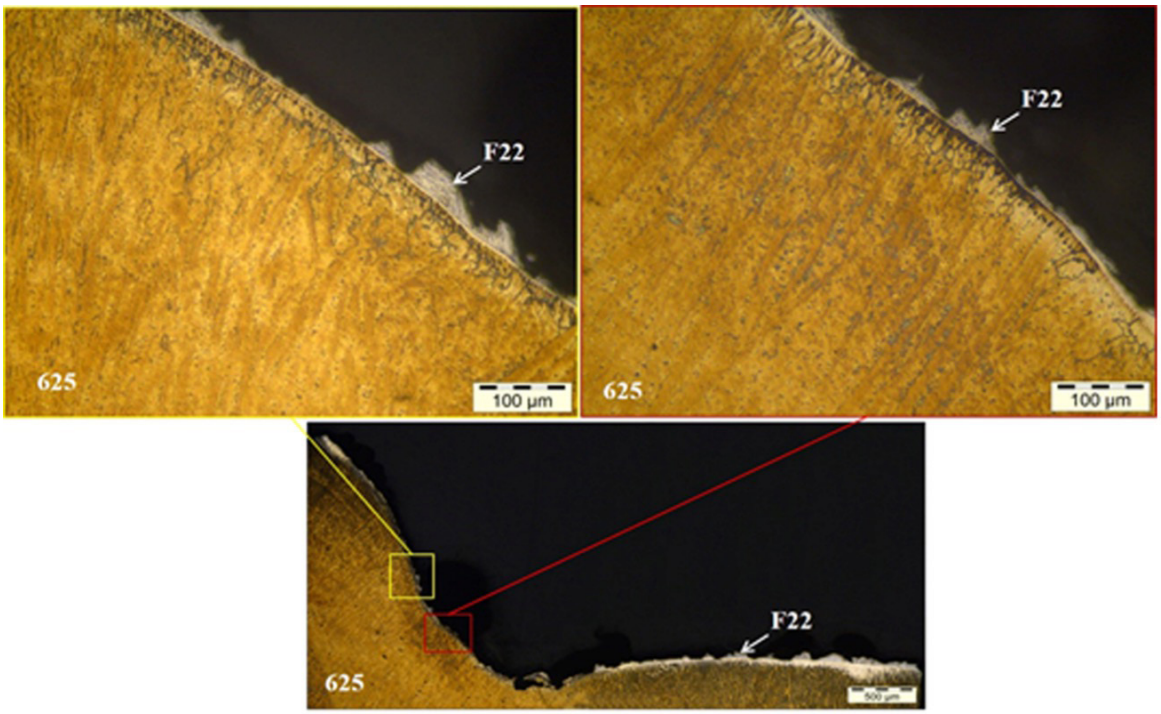


**Figure 16.** Optical microscopy of the cross section of the welded joint, steel ASTM A182 F22 - Inconel 625 - steel ASTM A36 with hydrogenation.

the fractured surface of the hydrogenated joint, a fragile fracture morphology was observed, with a predominance of the quasi-cleavage mechanism, Figure 15b.

Figure 16 shows the optical microscopy images of part of the cross section of the fracture surface of the hydrogenated welded joint. In the smallest scale image (500µm), the total width of the specimen is observed, after testing, and it is noted that, from the central region to the right end of this image, the rupture develops predominantly in the region of the HAZ, steel very close to the interface, which, as it was showed is the region where the PMZs occur, more specifically, the M and Δ zones. In the two images of greater magnification (100µm), it is possible to notice the occurrence of rupture predominantly close to the interface but on the steel side, that is, outside the ϕ zone. Thus, although some authors such as Dai and Lippold[20] attribute the fragile fracture mechanism mainly to the presence of the ϕ zone, the results obtained, with the fractures occurring in the steel region, suggests that the high hardness microfases of steel such as the M phase and the presence of carbides were more susceptible to hydrogen embrittlement. All specimens (SE(B)) of tested weld joints presented similar crack deviation behavior, regardless of the presence or absence of cathodic protection.

### *3.3. Fracture mechanics test*

The average curves, Force vs. Notch Opening Displacement (NOD) for the fracture mechanics tests, of the base metal, in the conditions without (OH) and with (WH) hydrogenation are shown in Figure 17. The characteristics of the crack tests fatigue and CTOD are shown in Table 12, for both conditions tested.

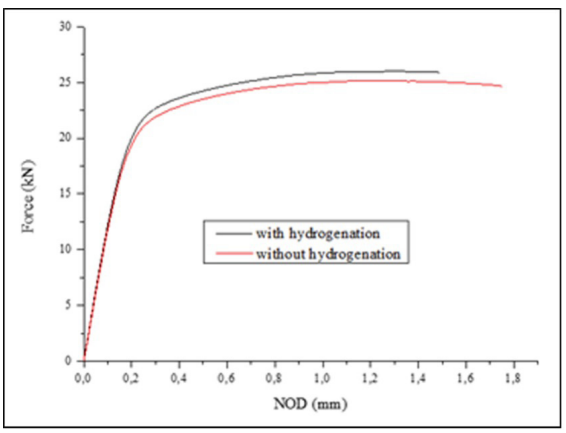


**Figure 17.** Average force vs. Notch-Opening Displacement curves for base metal, ASTM A182 F22 steel, without and with hydrogenation.

The average Force vs. NOD for the base metal, subjected to cathodic protection, is in line with that of the non-hydrogenated base metal, suggesting that the hydrogen did not affect the plastic behavior of the base metal, since the average values of CTOD and the plastic component, shown in Table 12, had insignificant variations. It is observed that the $\delta_m$ values showed a slight increase, of only 5%, for the hydrogenated condition. This behavior of hydrogen, by which it favors the plasticity of the material, may be related to the model of localized plasticity, and to the increased mobility of dislocation caused by the presence of hydrogen. According to Birnbaum and Sofronis[24], the hydrogen dissolved in

the crystalline network reduces the interactions between discordances, thus facilitating a greater flow of deformations.

In images of Figure 18a and b, we have the results of fractography of the base metal specimens without hydrogenation, whereas in images (c) and (d), of the same Figure, we have the results for the base metal with hydrogenation. The transversal surface of the analyzed specimens, being the regions of the fatigue crack (FC) and test crack (TC), highlighted by the dashed lines, are shown in Figure 18a and c.

The test crack of the base metal without hydrogenation verified in the SEM image of Figure 18b, shows a predominance of a ductile type fracture mechanism, which involves nucleation, growth and the microvoid coalescence (dimples). In some studies, this ductile fracture mode is identified as a ductile rupture zone, or extension of stable cracks, and is associated with the rounding process that occurs in front of the fatigue crack tip during the growth of the test crack[25]. In addition, other authors such as Fassina et al.[26], mention that second phase particles, such as precipitates and non-metallic inclusions and grain boundary, are sites of nucleation of these microvoids. In this respect, through Figure 18b, there are formations (dashed squares) suggestive of these inclusions

**Table 12.** Results of CTOD tests of the base metal, ASTM A182 F22 steel, without (OH) and with (WH) hydrogenation.

| Condition | Specimen | Fatigue crack | | | Stress intensity factor | CTOD | | |
|---|---|---|---|---|---|---|---|---|
| | | Nº of cycles | $a_0$ (mm) | $a_0/W$ | g ($a_0/W$) | $V_P$ (mm) | Force (kN) | $\delta_m$ (mm) |
| OH | 1 | 95985 | 10.13 | 0.507 | 2.72 | 0.63785 | 25.1880 | 0.23000 |
| | 2 | 71860 | 10.32 | 0.516 | 2.80 | 0.88848 | 25.1130 | 0.29619 |
| | 3 | 65005 | 10.18 | 0.509 | 2.74 | 0.95274 | 24.9870 | 0.31906 |
| | **Average** | | | | | **0.82636** | **25.0960** | **0.28175** |
| WH | 1 | 61812 | 10.04 | 0.502 | 2.68 | 0.94721 | 26.0295 | 0.32404 |
| | 2 | 61757 | 10.03 | 0.501 | 2.68 | 0.75913 | 25.7855 | 0.26636 |
| | 3 | 64960 | 10.02 | 0.501 | 2.67 | 0.85812 | 26.0600 | 0.29724 |
| | **Average** | | | | | **0.85482** | **25.9583** | **0.29588** |

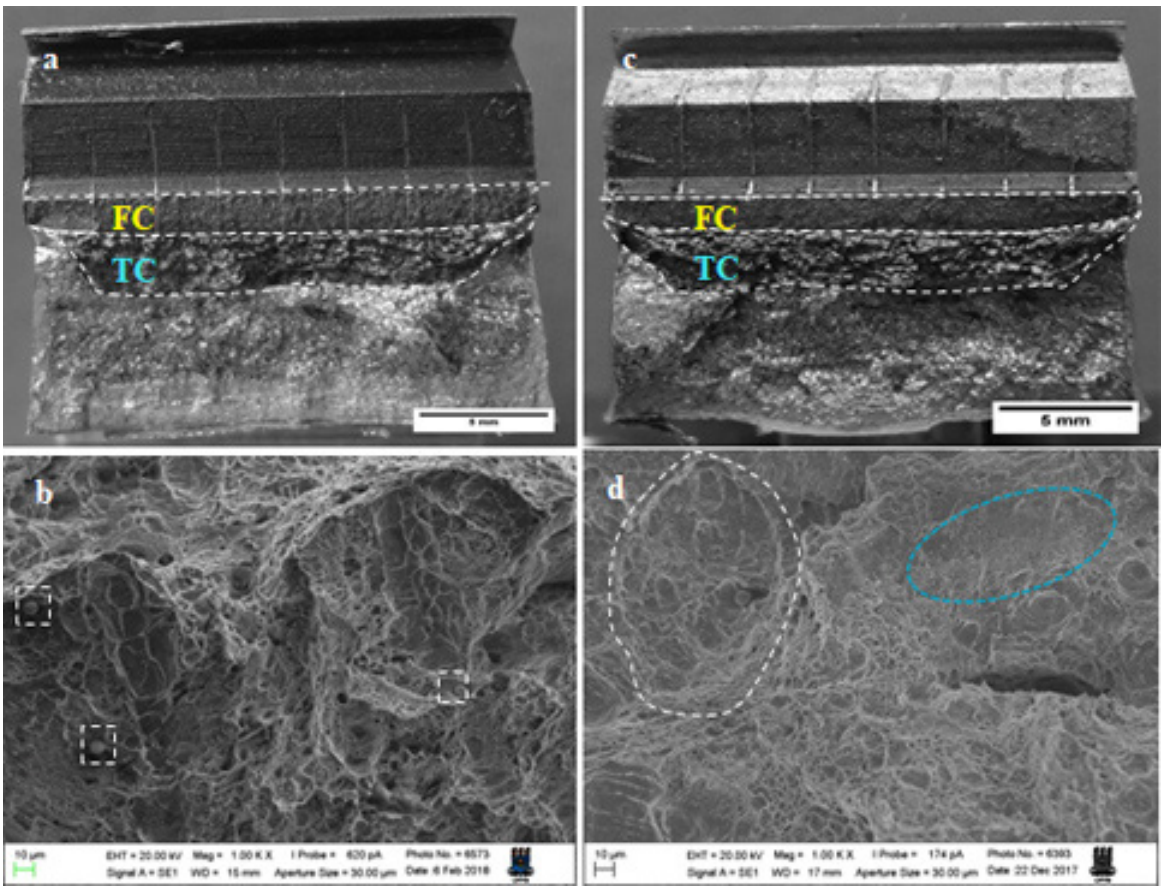


**Figure 18.** Fractography of ASTM A182 F22 steel. (a) transverse surface and (b) SEM (1000x) without hydrogenation. (c) transverse surface and (d) SEM (1000x) with hydrogenation.

located within the microvoids. Considering the chemical composition of ASTM A182 F22 steel, it can be associated, for example, that in these inclusions there are carbides, rich in Cr and Mo, which correspond to the alloying elements in greater proportions.

With respect to the hydrogenated base metal, SEM image of Figure 18d, a formation that resembles the "cellular" type (dashed line) is observed, which is mentioned by the authors Fassina et al.[26] when studying the ASTM A 182 F22 steel. This type of formation is characterized, in most cases, by the presence of inclusions in its interior and mixed fracture mechanism, characterized by a fragile mode in the central part of the cell and a ductile mode at the border. The "cellular" formation, seen in Figure 18d, has dimensions of approximately 70x110µm, very close to the results found by Fassina et al.[23].

Dai and Lippold[27] presented several failure morphologies of the welded joint ASTM A182 F22 and Inconel 625, among which the microvoid coalescence (MVC) and quasi-cleavage (QC), which are Hydrogen Assisted Cracking (HAC) morphologies, common in ASTM A182 F22 steel, according to Beachem's theory. The morphologies presented in Figure 18d suggest the presence of a mixed failure mechanism, involving dimples, MVC (white dashed line) and QC (blue dashed line), that is, a combination between the fragile and ductile mechanisms, with predominance of this last. Combining the results of CTOD and fractography, there is little role of hydrogen in the process of steel embrittlement, under the processing conditions that were used.

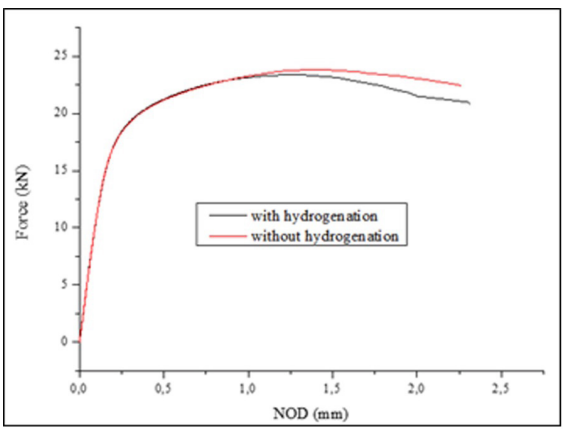


**Figure 19.** Average force vs. Notch-Opening Displacement curves of the welded joint notch without and with hydrogenation.

Figure 19 shows the average Force curves vs. NOD for ASTM A182 F22 dissimilar welded joint - Inconel 625 - ASTM A36 steel, without and with hydrogenation. Regarding the plastic behavior of these curves, it appears that this was also consistent with the failure mode in terms of $\delta_m$, Table 13, similar to what was seen for the base metal.

When comparing the average values ($\delta_m$) for the conditions without and with hydrogenation, it is observed that the welded joint ASTM A182 F22 steel - Inconel 625 - ASTM A36 steel had the fracture toughness reduced by approximately 16%, thus demonstrating susceptibility to hydrogen embrittlement. This embrittlement effect, induced by the hydrogen of the welded joint, was also evidenced by the failure mechanisms presented below. It is worth noting that the test in an assisted environment and at a low deformation rate is more effective in determining susceptibility to embrittlement[28]; so, if we consider that the tests carried out were quasistatic and in air, it is believed that the susceptibility to embrittlement of the developed welded joint tends to be more pronounced.

In images of Figure 20a and b we have the results of fractography of the welded joint specimens without hydrogenation, whereas in images (c) and (d), of the same Figure, we have the results for the hydrogenated welded joint. The transversal surface of the analyzed specimens, whose regions of the fatigue crack (FC) and test crack (TC) are highlighted by the dashed lines, are shown in Figure 20a and c.

In the SEM image of Figure 20b, there are test crack regions of the welded joint without hydrogenation, which behaved similarly to the base metal (Figure 19b), the failure mechanism being predominantly ductile via dimples.

From Figure 20d, it appears that the fractured surface of the hydrogenated welded joint has a mixed failure mechanism, including MVC (white circles), QC (blue circle) and dimples. With the exception of the last mechanism, the others are associated with HAC. Considering the nomenclature adopted by Fassina et al.[26], the white circles are similar to the "cellular" formation.

Finally, it is evident that both the results of fractography and those of CTOD, of welded joints without and with hydrogenation, indicate the tendency of embrittlement in the

**Table 13.** Results of CTOD tests of the welded joint, steel ASTM A182 F22 - Inconel 625 - steel ASTM A36, without (OH) and with (WH) hydrogenation.

| Condition | Specimen | Fatigue crack | | | Stress intensity factor | CTOD | | |
|---|---|---|---|---|---|---|---|---|
| | | Nº of cycles | $a_0$ (mm) | $a_0/W$ | g ($a_0/W$) | $V_P$ (mm) | Force (kN) | $\delta_m$ (mm) |
| OH | 1 | 65406 | 10.17 | 0.508 | 2.73 | 1.10467 | 23.6880 | 0.36137 |
| | 2 | 55854 | 9.96 | 0.498 | 2.64 | 1.09830 | 24.1425 | 0.36826 |
| | 3 | 74537 | 10.07 | 0.503 | 2.69 | 1.10343 | 23.7390 | 0.36539 |
| | **Average** | | | | | **1.14099** | **23.8930** | **0.36501** |
| WH | 1 | 69578 | 10.19 | 0.509 | 2.74 | 0.96371 | 22.9415 | 0.31674 |
| | 2 | 53546 | 10.02 | 0.501 | 2.67 | 0.99787 | 23.9835 | 0.33468 |
| | 3 | 63645 | 10.07 | 0.503 | 2.69 | 0.88485 | 23.5900 | 0.29786 |
| | **Average** | | | | | **0.94881** | **23.5050** | **0.31643** |

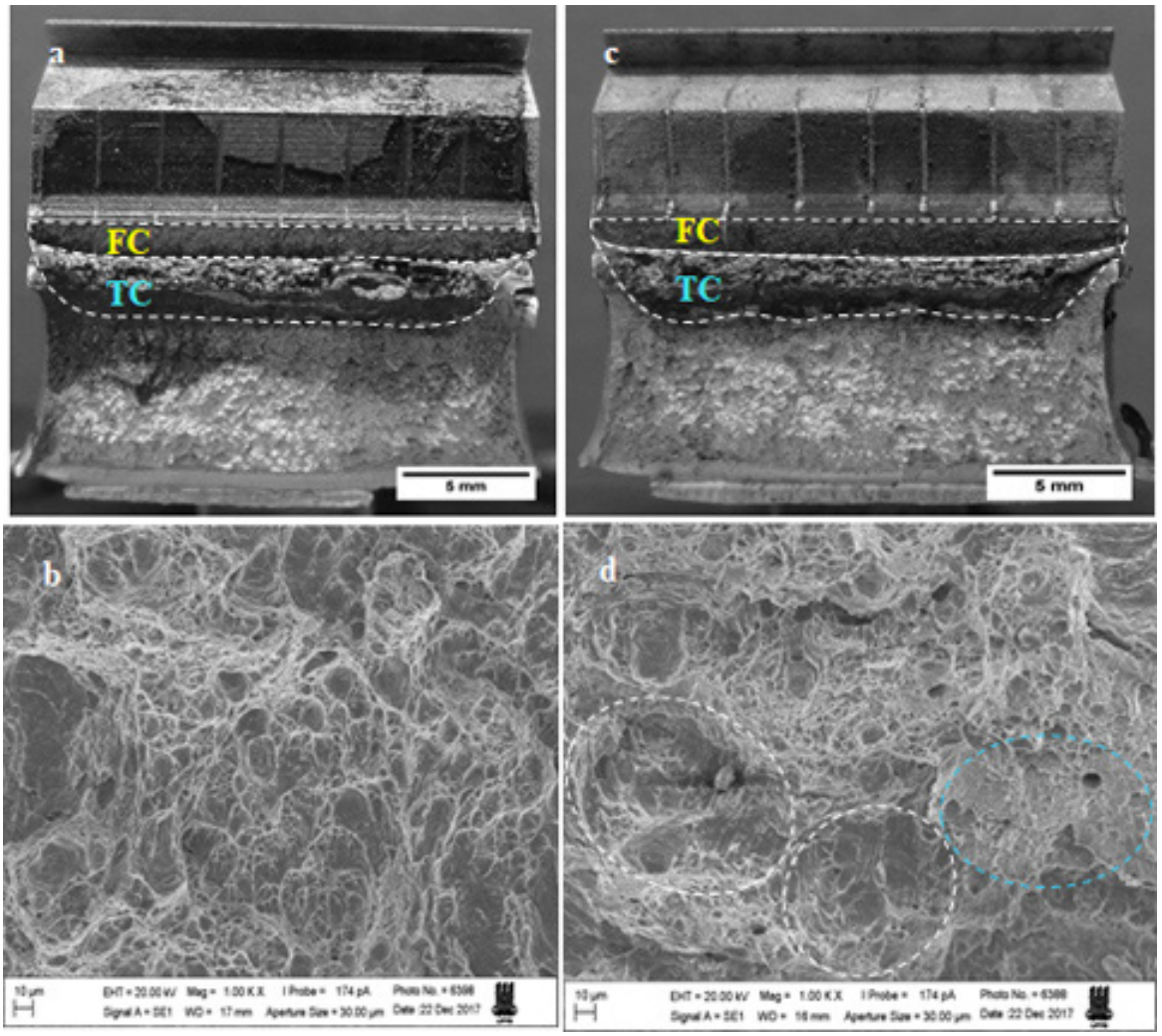


**Figure 20.** Fractography of the welded joint. (a) transverse surface and (b) SEM (1000x) without hydrogenation. (c) transverse surface and (d) SEM (1000x) with hydrogenation.

welded joint, associated with the base metal HAZ. Additionally, even with this embrittlemnet indicator, the presence of "pop_--in" was not observed, as well as no discontinuity in the F curves vs. NOD, which reinforces the fact that the presence of dissolved hydrogen in the crystalline network reduced the interactions between dislocations, promoting an increase in the plastic deformation in front of the crack, that is, thus facilitating a greater flow of deformations[24].

In Figure 21, there is an analysis of the deviation between the fatigue and the test crack, using optical microscopy. This analysis serves as a support to better locate the development region of the test crack. The specimens were analyzed under the conditions without (Figure 21a and b) and with (Figure 21c and d) cathodic protection. All specimens (SE (B)) of tested welded joints showed similar crack deviation behavior, regardless of the presence or absence of cathodic protection.

Figure 21a shows the fatigue crack (horizontal red line), which remained flat, and at 1.1 mm from the LF (vertical red line). Still in this Figure, it is possible to observe the beginning of the test crack, which, in relation to the fatigue crack, has a slight deviation. In Figure 21b, there is the continuity of this crack that was maintained in the HAZ region. However, it is possible to observe a more pronounced deviation when it approaches the fusion line, with strong indications that it does not reach or exceed the weld metal.

Images of Figure 21c and d, in turn, show the images of the crack deviation of the hydrogenated welded joint specimens. In Figure 21c, it is noted that the fatigue crack (horizontal red line) also remained flat, with a length close to approximately 1.2 mm (vertical red line), from the fusion line. Still with respect to Figure 21c, it appears that the test crack deviated slightly in relation to the fatigue crack. Such an occurrence is a strong indication that the hydrogenation process did not influence the direction of its development, that is, the result is similar to that of the material without hydrogenation.

The average values and standard deviation of the CTOD ($\delta_m$), presented in Tables 12 and 13, for the base metal and welded joint, both in the conditions without (MF22S and

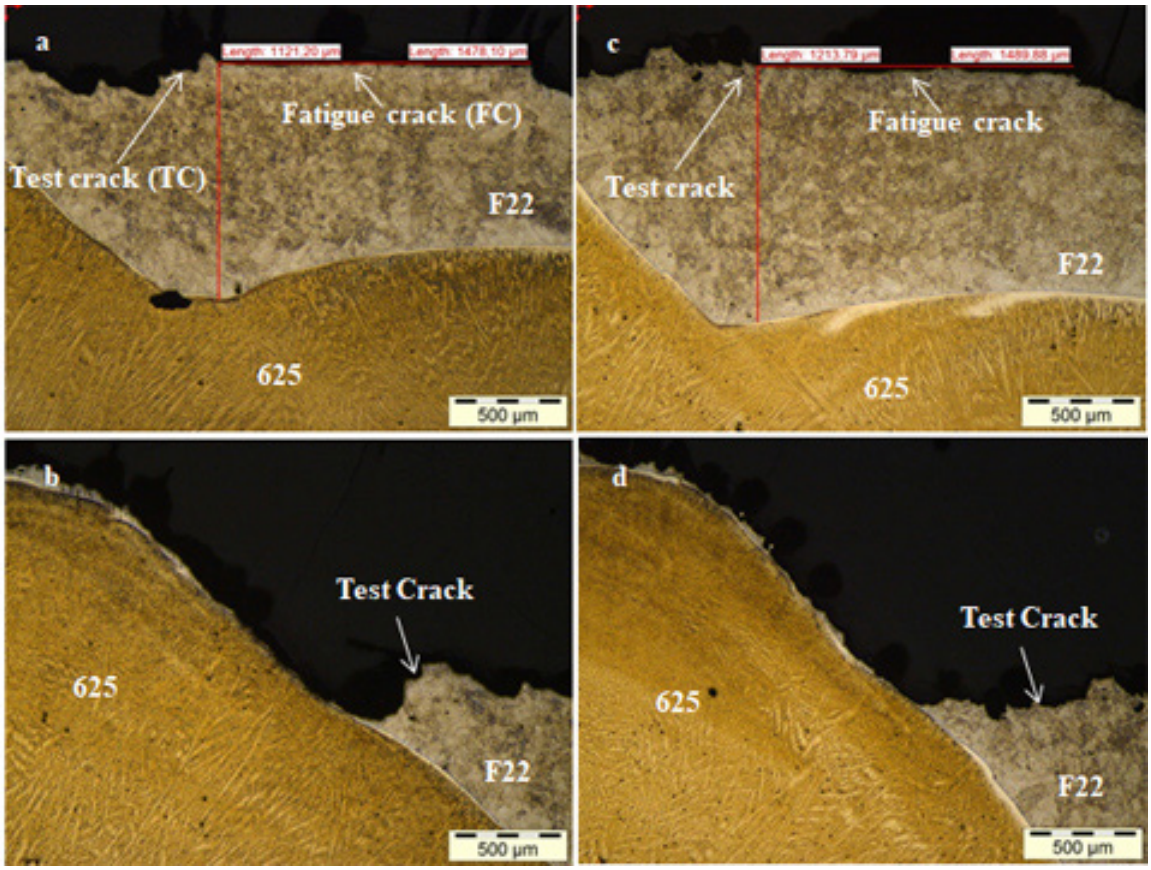


**Figure 21.** Fatigue cracks optical microscopy and testing of welded joint CTOD specimens, steel ASTM A182 F22 - Inconel 625 - steel ASTM A36(increase of 50x). (a) and (b) without hydrogenation. (c) e (d) with hydrogenation.

MJSS) and with (MF22H and MJSH) hydrogenation, are also presented in the chart of Figure 22. Considering the standard deviation, it is evident that the reduction of fracture toughness of hydrogenated BM (yellow and green columns) has not been clearly proven. Regarding the welded joint (blue and gray columns), it is noted that, regardless of the standard deviation, the hydrogenated joint was susceptible to hydrogen embrittlement. This susceptibility to the embrittlement of the welded material suggests a direct relationship with the welding parameters and PWHT employed, responsible for the presence of the PMZs at the dissimilar interface. When we consider the fact that the fatigue crack is 1 mm from the LF, which has a hardness close to 246$HV_{0.1}$, while the point microhardness values of zone M (Figure 10 and Table 9) were higher than 400$HV_{0.1}$, it should be considered that: the use of a fatigue crack closer to the interface could provide a greater hydrogen trapping, in this interface, with greater hardness, and, thus, favor a greater reduction in the CTOD value of the welded joint.

Comparing the results of fracture mechanics with those of tensile test it was observed that the fatigue crack in the CTOD test was developed in the HAZ, but far from the PMZs, without including the M zones, and the hydrogen embrittlement was not as intense, as in the case of the tensile test, in which the entire weld interface, containing all regions of the PMZs and high hardness M zones, was subjected to tensile efforts.

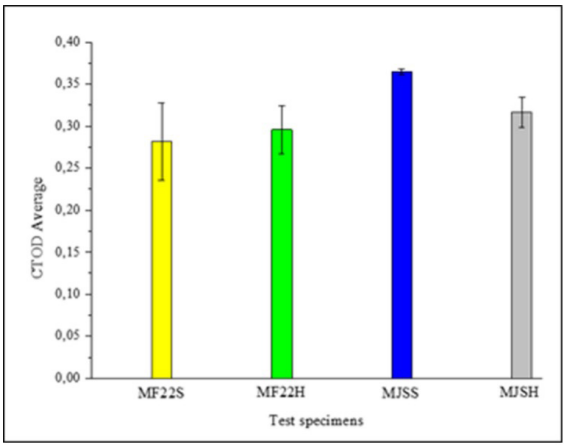


**Figure 22.** Average and standard deviation of CTOD results (δ) for the four conditions tested.

## 4. Conclusions

In this study, it was researched the influence of hydrogen on the mechanical properties of ASTM A182 F22 steel and the dissimilar welded joint, consisting of the base metals (BMs) ASTM A182 F22 steel / ASTM A36 steel and weld metal (WM) Inconel 625, which was analyzed in the conditions without and with previous hydrogen loading. Therefore,

based on the research developed and here within presented, the main conclusions are that:

1. ASTM A182 F22 steel, subjected to previous hydrogenation, was not susceptible to hydrogen embrittlement, maintaining the same plasticity and ductile fracture characteristic of tensile tests without the presence of hydrogen.
2. The welded joints of ASTM A182 F22 steel with ASTM A 36 steel, using Inconel 625 as a filler and buttering metal, showed a significant sensitivity to hydrogen embrittlement, reducing elongation by 15% and reduction of area by 56%, in tensile tests, maintaining the levels of yield and tensile strength.
3. The toughness test results showed that the ASTM A182 F22 stell, had a low sensibility to hydrogen embrittlement while the ASTM A182 F22 steel welded joint - Inconel 625 - ASTM A36 steel, showed a reduction of 13.3% in the value of the CTOD for the samples submitted to hydrogenation.
4. All fractures of the welded joints in the tensile and CTOD tests occurred in the ASTM A182 F22 steel HAZ, which had partially mixed zones rich in martensite (M regions), with microhardness values around 400 HV.
5. The fracture morphology of the base metals specimens and welded joints, without hydrogenation, indicated the predominance of the ductile mechanism, both in the tensile tests and in the fracture mechanics. In hydrogenated specimens, a mixed mechanism was observed in the tensile tests, with the presence of mechanisms by dimples and transgranular cleavage, whereas, in the fracture mechanics tests, the presence of the MVC, QC and dimples mechanisms was evident.

## 5. Acknowledgements

The authors would like to thank Prof. Dr. Severino Jackson Guedes de Lima (in memorium) for all the legacy left to the Postgraduate Programs in Mechanical Engineering and in Materials Science and Engineering at the Federal University of Paraíba, whose present work is included.

## 6. References

1. Dodge MF, Gittos MF, Dong H, Zhang SY, Kabra S, Kelleher JF. In-situ neutron diffraction measurement of stress redistribution in a dissimilar joint during heat treatment. Mater Sci Eng A. 2015;627:161-70. http://dx.doi.org/10.1016/j.msea.2014.12.095.
2. Zhou C, Huang Q, Guo Q, Zheng J, Chen X, Zhu J, et al. Sulphide stress cracking behaviour of the dissimilar metal welded joint of X60 pipeline steel and Inconel 625 alloy. Corros Sci. 2016;110:242-52. http://dx.doi.org/10.1016/j.corsci.2016.04.044.
3. Kulkarni A, Dwivedi DK, Vasudevan M. Dissimilar metal welding of P91 steel-AISI 316L SS with Incoloy 800 and Inconel 600 interlayers by using activated TIG welding process and its effect on the microstructure and mechanical properties. J Mater Process Technol. 2019;274:116280. http://dx.doi.org/10.1016/j.jmatprotec.2019.116280.
4. Rathod DW, Singh PK, Pandey S, Aravindan S. Effect of buffer-layered buttering on microstructure and mechanical properties of dissimilar metal weld joints for nuclear plant application. Mater Sci Eng A. 2016;666:100-13. http://dx.doi.org/10.1016/j.msea.2016.04.053.
5. Klapper HS, Klöwer J, Gosheva O. Hydrogen embrittlement: the game changing factor in the applicability of nickel alloys in oilfield technology. Philos Trans R Soc A Math Phys Eng Sci. 2017;375(2098):1-10. http://dx.doi.org/10.1098/rsta.2016.0415.
6. Fenske JA. Microstructure and hydrogen induced failure mechanisms in iron-nickel weldments. Urbana: University of Illinois at Urbana-Champaign; 2010.
7. Olden V, Kvaale PE, Simensen PA, Aaldstedt S, Solberg JK. The effect of PWHT on the material properties and micro structure in inconel 625 and inconel 725 buttered joints. In: Proceedings of OMAE 2003: The 22nd International Conference on Offshore Mechanics & Arctic Engineering; 2003; Cancun. New York: ASME; 2003. p. 1-7.
8. de Oliveira GLG. Soldagem dissimilar dos aços AISI 8630M e ARTM A182 F22 para aplicações subaquáticas [thesis]. Fortaleza: Universidade Federal do Ceará; 2013 [cited 2021 Jul 5]. Available from: http://www.repositorio.ufc.br/handle/riufc/7804
9. Dodge MF. The effect of heat treatment on the embrittlement of dissimilar welded joints. United Kingdom: University of Leicester; 2014.
10. ASTM International. ASTM E8/E8M. Standard Test Methods for Tension Testing of Metallic Materials. West Conshohocken, PA: ASTM International; 2009. p. 1-27.
11. Silva AN. Análise do efeito do hidrogênio na resposta de tenacidade à fratura em junta soldada dissimilar [thesis]. João Pessoa: Universidade Federal da Paraíba; 2018.
12. British Standards. BS EN ISO 15653. Metallic materials — method of test for the determination of quasistatic fracture toughness of welds. United Kingdom: British Standards; 2010.
13. ASTM International. ASTM D1141-98. Standard Practice for the Preparation of Substitute Ocean Water. West Conshohocken, PA: ASTM International; 2013.
14. Beaugrand VCM, Smith LS, Gittos MF. Hydrogen embrittlement of 8630M/625 subsea dissimilar joints: factors that influence the performance. In: Proceedings of the 28th International Conference on Ocean, Offshore and Arctic Engineering; 2009; Honolulu, Hawaii, USA. New York: ASME; 2009. p. 1-10.
15. Dodge MF, Dong HB, Gittos MF, Mobberley T. Fusion zone microstructure associated with embrittlement of subsea dissimilar joints. In: Proceedings of the ASME 2014 33rd International Conference on Ocean, Offshore and Arctic Engineering; 2014; San Francisco, California, USA. New York: ASME; 2014. p. 1-11.
16. Bourgeois D. Hydrogen assisted crack in dissimilar metal welds for subsea service under cathodic protection. Ohio: Ohio State University; 2015.
17. Fenske JA, Robertson IM, Ayer R, Hukle M, Lillig D, Newbury B. Microstructure and hydrogen-induced failure mechanisms in Fe and Ni alloy weldments. Metall Mater Trans A. 2012;43:3011-22. http://dx.doi.org/10.1007/s11661-012-1129-1.
18. Silva AN, Costa EC, Silva RDS, Almeida JG, Lima SJG, Passos TA. Butter-weld interface microstructural analysis employing NCS and LAMS sections. Mater Res. 2019;22:1-13. http://dx.doi.org/10.1590/1980-5373-MR-2019-0018.
19. Frei J, Alexandrov BT, Rethmeier M. Low heat input gas metal arc welding for dissimilar metal weld overlays part II: the transition zone. Weld World. 2017;62(3):317-24. http://dx.doi.org/10.1007/s40194-017-0539-5.
20. Dai T, Lippold JC. The effect of postweld heat treatment on hydrogen-assisted cracking of F22/Alloy 625 overlays. Weld J. 2018;97:75s-90s. http://dx.doi.org/10.29391/2018.97.007.
21. Fenske JA, Hukle MW, Newbury B, Gordon JR, Noecker R, Robertson IM. Hydrogen induced mechanical property behavior of dissimilar weld metal interfaces. In: Proceedings of the ASME

2011 30th International Conference on Ocean, Offshore and Arctic Engineering OMAE2011; 2011; Rotterdam. New York: ASME; 2011. p. 1-8.

22. NACE International. NACE MR0175. Petroleum and natural gas industries - Materials for use in H2S-containing environments in oil and gas production. USA: NACE International; 2003.
23. Fassina P, Bolzoni F, Fumagalli G, Lazzari L, Vergani L, Sciuccati A. Influence of hydrogen and low temperature on pipeline steels mechanical behaviour. Procedia Eng. 2011;10:3226-34. http://dx.doi.org/10.1016/j.proeng.2011.04.533.
24. Birnbaum HK, Sofronis P. Hydrogen-enhanced localized plasticity--a mechanism for hydrogenrelated fracture. Mater Sci Eng A. 1994;A176:191-202.
25. Hausild P, Nedbal I, Berdin C, Prioul C. The influence of ductile tearing on fracture energy in the ductile-to-brittle transition temperature range. Mater Sci Eng A. 2002;335:164-74. http://dx.doi.org/10.1016/S0921-5093(01)01913-X.
26. Fassina P, Brunella MF, Lazzari L, Re G, Vergani L, Sciuccati A. Effect of hydrogen and low temperature on fatigue crack growth of pipeline steels. Eng Fract Mech J. 2013;103:10-25. http://dx.doi.org/10.1016/j.engfracmech.2012.09.023.
27. Dai T, Lippold JC. Tempering effect on the fusion boundary region of alloy 625 weld overlay on 8630 steel. Weld World. 2018;62:535-50. http://dx.doi.org/10.1007/s40194-018-0560-3.
28. Gittos MF. Resistance of dissimilar joints between steel and nickel alloys to hydrogenassisted cracking. New Orleans: NACE International; 2008. p. 19.